

Electron acceleration at merger shocks of galaxy clusters in generalized hybrid kinetic simulations

Stella S. Boula,^{a,*} Jacek Niemiec,^a Takanobu Amano^b and Oleh Kobzar^c

^a*Institute of Nuclear Physics Polish Academy of Sciences, PL-31342 Krakow, Poland*

^b*Department of Earth and Planetary Science, University of Tokyo, 7-3-1 Hongo, Bunkyo-ku, Tokyo 113-0033, Japan*

^c*Cracow University of Technology, PL-30084 Kraków, Poland*

E-mail: stboula@ifj.edu.pl

Cosmic ray acceleration to high energies in galaxy clusters is still an open question. Relativistic electrons are produced at merger shocks, forming the so-called radio relics that emit synchrotron radiation. These large-scale shocks are also considered to be sources of high-energy cosmic rays and associated gamma-rays and neutrinos. We report on our recent studies of electron acceleration at merger shocks that have low Mach numbers and propagate in hot intracluster medium. Our recent PIC simulation results show that in these conditions, electron acceleration can be provided by the process of stochastic shock-drift acceleration that is facilitated through multi-scale turbulence in the shock, including the ion-scale shock surface rippling. Building upon these studies here we present results obtained with a newly developed generalized fluid-particle hybrid numerical code that can treat fluid electrons and ions, and an arbitrary number of kinetic species, including energetic particles. We discuss the structure of quasi-perpendicular shocks obtained in a standard hybrid simulation model with fluid electrons and kinetic ions. We show results of large-scale 2D simulations for the range of parameters, such as the plasma beta, the magnetic field obliquity angle, and the shock Mach number, including subcritical and supercritical conditions.

38th International Cosmic Ray Conference (ICRC2023)
26 July - 3 August, 2023
Nagoya, Japan



*Speaker

1. Introduction

Galaxy clusters are vast assemblies of galaxies, hot gas, and dark matter that are gravitationally bound together. Observations of radio relics in radio and X-rays has provided compelling evidence for the acceleration of relativistic electrons at merger shocks within galaxy clusters [1]. The most energetic merger shocks have low sonic Mach numbers, $M_s \leq 5$, and propagate in a hot intracluster medium (ICM) characterized by a high plasma beta, $\beta \gg 1$, which is the ratio of thermal to magnetic pressures. Diffusive Shock Acceleration (DSA) is commonly invoked as the mechanism responsible for particle acceleration. However, an essential element of this process involves the electron injection mechanism, which remains inadequately understood for ICM conditions. Among the extensively debated electron injection mechanisms at ICM shocks, Shock Drift Acceleration (SDA) [2] has gained attention [2]. Recent investigations with particle-in-cell (PIC) simulations have shed light on the fact that electrons, when reflected from the shock during the SDA process, have the potential to instigate turbulence in the upstream region of the shock [3–6]. These waves are driven by electron firehose instability (EFI) and can scatter electrons back towards the shock, facilitating further interaction with the shock. It has been confirmed that this multiple-cycle SDA process can lead to the formation of supra-thermal electron spectra upstream and operates efficiently in high-beta shocks. However, the maximum energies achieved are smaller than the estimated injection threshold for DSA. Large-scale PIC simulations of a quasi-perpendicular subluminal shocks [7, 8] have recently shown that the primary pre-acceleration mechanism for electrons up to the injection energy is the stochastic SDA (SSDA) [9]. In SSDA, electrons undergo stochastic pitch-angle scattering off multi-scale waves and stay confined for an extended time in the shock transition, gaining the energy via the gradient drift. A critical factor for SSDA is the presence of wide-band turbulence, including long-wave shock rippling, associated with ion kinetic instabilities arising from temperature anisotropies.

While fully kinetic PIC simulations are restricted to a narrow range of temporal and spatial scales, hybrid kinetic simulations, incorporating kinetic ions and fluid electrons, can treat extensive macroscopic systems and therefore be of great value in expanding our understanding of ion DSA and ion-scale turbulence in non-relativistic shocks. A combined hybrid kinetic and test-particle model has been recently employed to study two- and three-dimensional (2D and 3D) turbulent structure of low Mach number shocks in low-beta plasmas and the electron acceleration therein [10]. In this paper we present preliminary results of our new 2D hybrid simulations that investigate a range of high plasma beta, sonic Mach numbers, and the shock obliquity angles on spatial and temporal scales that allow the development of large-scale turbulence modes in the system. This initial analysis serves as a base for further exploration of the merger shock physics with 3D simulations.

2. Numerical setup

Our study utilizes a generalized fluid-particle hybrid numerical code [11] that treats the collisionless plasma under the assumption of quasi-neutrality. The model consists of fluid ions and electrons and an arbitrary number of kinetic species. The dynamics of fluid and kinetic populations are coupled together in a self-consistent manner. The code employs the exact form of the generalized Ohm's law, which allows us to consider arbitrary mass and energy densities, as well as

the charge-to-mass ratio of the kinetic species. Here, we consider fluid electrons and kinetic ions, resembling a standard hybrid model, but with proper treatment of finite electron inertia effects. We assume the ion-to-electron mass ratio $m_i = 100 m_e$.

In our 2D simulations, an electron-ion plasma beam is injected at the right side of the computational box in the $x - y$ plane and flows with a bulk velocity u_0 in the $-x$ -direction. The collision of the inflowing plasma with the beam reflected off the conductive wall at the left boundary spawns a shock propagating in the $+x$ -direction with velocity u_{sh} , as measured in the upstream rest frame. The injected plasma carries a large-scale magnetic field, B_0 , which lies in the simulation plane and is inclined at the angle θ_{Bn} to the shock normal. We study quasi-perpendicular shocks, for which $\theta_{Bn} > 45^\circ$. We simulate shocks with sonic Mach number $M_s = u_{sh}/c_s = 3$ in a range of total plasma beta $\beta = \beta_e + \beta_i = 8\pi(N_e + N_i)k_B T_0/B_0^2 = 3 - 50$, that initially is equally carried by the electrons and ions, $\beta_e = \beta_i$. Here, c_s is the sound velocity and $N_e = N_i$ the electron/ion number density. We also perform simulations in a range of sonic Mach numbers $M_s = 2 - 4$ and plasma beta, and investigate the role of the obliquity angle in the case of $\beta = 10$ for $\theta_{Bn} = 55^\circ - 89^\circ$.

Our unit of space is the ion skin depth $\lambda_i = \sqrt{4\pi e^2 N_i/m_i}$ or the ion gyroradius $r_g \equiv u_0/\Omega_i = u_0/u_{sh} M_s \lambda_i \sqrt{\beta\Gamma/2}$, where e is the electric charge, m_i the ion mass, and $\Gamma = 5/3$ is the adiabatic index. The time unit is the ion gyrofrequency $\Omega_i = eB_0/m_i$. The time step $\delta t = 10^{-3} \Omega_{ci}^{-1}$. We resolve λ_i with 4 cells and use $N_{ppc} = 128$ particles per cell. The transverse size of the simulation box is several r_g , to resolve large-scale shock ripple modes.

3. Results

3.1 Structure of $M_s = 3$ shocks and comparison with PIC simulations

Figure 1 shows a typical structure of an evolved quasi-perpendicular subluminal shock for the example case of $M_s = 3$, $\beta = 10$, and $\theta_{Bn} = 75^\circ$. The ion density map and profile show a familiar structure of overshoot-undershoot oscillations at the shock. The density compression relaxes far downstream to the Rankine-Hugoniot value of ~ 3 . This structure is due to the reflection of a portion of the incoming ions back upstream, as evidenced by ions with large positive v_{xi} and v_{zi} in the phase-space ahead of the shock at $x/\lambda_i \approx 64$ (Fig. 1b). The ion reflection causes a strong ion temperature anisotropy, $T_\perp/T_\parallel \gg 1$, at the shock ramp and overshoot, which is the source of strong magnetic fluctuations, visible in the magnetic field maps and profiles in Figure 1a and 1c. Their amplitude at the shock is large enough to cause deviations from the frozen-in prediction, as traced by the density profile. The temperature anisotropy diminishes with a distance from the shock front, while T_\parallel increases. This demonstrates that ions are scattered off turbulence, which leads to isotropization of their distribution.

The magnetic waves in the shock at $x/\lambda_i \approx 35 - 65$ in B_x and B_y components are consistent with the Alfvén Ion Cyclotron (AIC) instability-generated turbulence. Their wavenumbers at the shock front are nearly aligned with the background compressed field. In addition, compressional components observed mainly in the B_y magnetic field can be identified with the ion mirror modes, whose wavenumbers are oblique. To validate the wave identification we have performed the linear analysis calculations, assuming a bi-Maxwellian ion velocity distribution function. The model is similar to that used in [12], but we approximate numerical values at the overshoot with $T_\perp/T_\parallel = 4$, rather

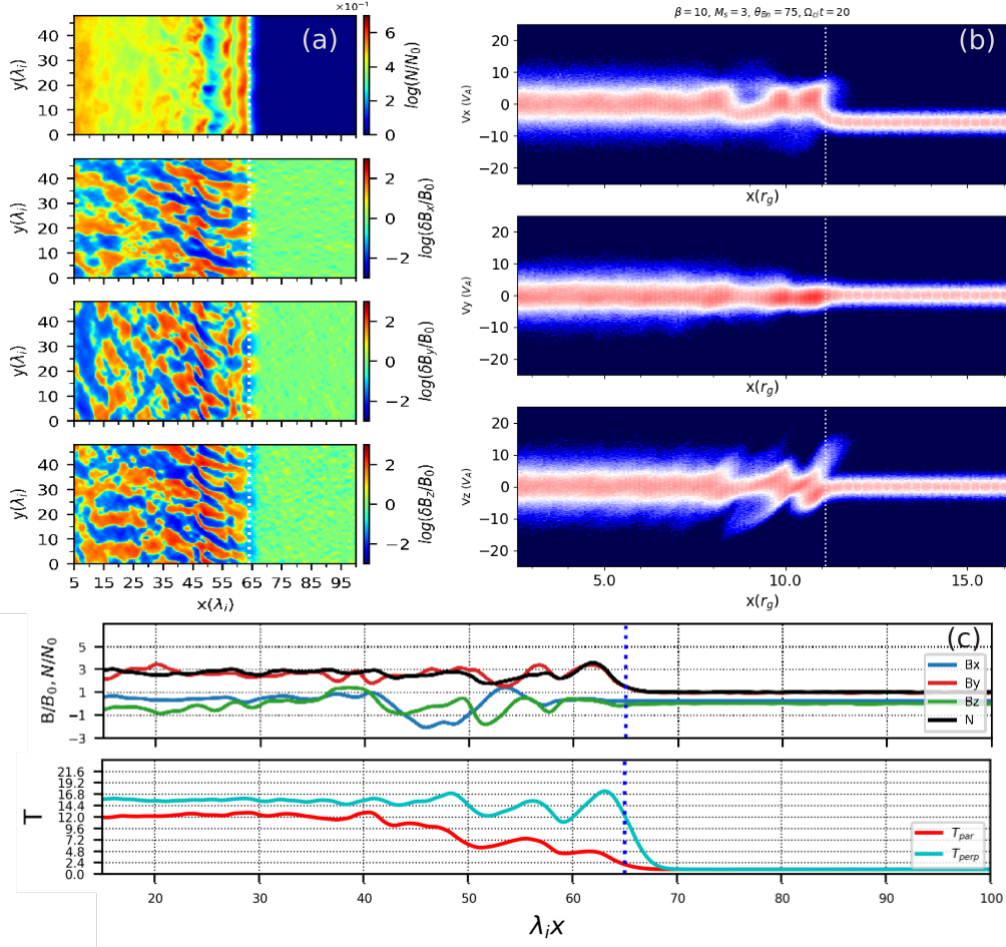


Figure 1: Shock structure at time $t = 20\Omega_{ci}^{-1}$ for the case of $M_s = 3$, $\beta = 10$, and $\theta_{Bn} = 75^\circ$. Panel a) shows maps of the normalized ion density, N_i/N_{0i} , and the normalized magnetic fluctuations, in which the magnitude of the frozen-in magnetic field is subtracted: $\delta B_x = B_x - B_0 \cos \theta_{Bn}$, $\delta B_y = B_y - B_0 \sin \theta_{Bn} (N_i(x)/N_{0i})$, $\delta B_z = B_z$, where $N_i(x)$ is the y -averaged ion density. The scaling is logarithmic and for the magnetic fields, it is sign-preserving, e.g., for δB_z it is: $\text{sgn}(\delta B_z) \cdot \{2 + \log[\max(|\delta B_z|/B_0, 10^{-2})]\}$. The level of "0" on the color scale hence corresponds to $|\delta B|/B_0 \leq 10^{-2}$ [see, e.g., 7]. Panel b) shows ion velocity phase-space, $x - \mathbf{v}_i$, and Panel c) the y -average profiles of density, magnetic field components, and the temperature components parallel and perpendicular to the local magnetic field). Vertical dotted line marks the shock position.

than taking their average over a more extended shock transition zone. For plasma beta in a range $\beta \approx 5 - 20$, the fastest growth occurs at parallel wavevector component $k_{\parallel} \lambda_i \approx 1.3$, corresponding to a wavelength of $\sim 5\lambda_i$, and moves slightly towards shorter wavevectors at higher β . One can compare this estimate with wavelengths observed in the region of the overshoots in the δB_z magnetic field map in the right panel of Figure 2, which shows the structure of a $M_s = 3$ and $\beta = 5$ shock at time $t\Omega_{ci} = 12$ close to the linear stage. The observed wavelength $\lambda_{AIC} \approx 5\lambda_i$ closely matches the calculated one.

Figure 2 compares results for the same shock parameters obtained with PIC (left, [7]) and hybrid (right) simulations. In PIC simulations, the electron whistler waves dominate the turbulence

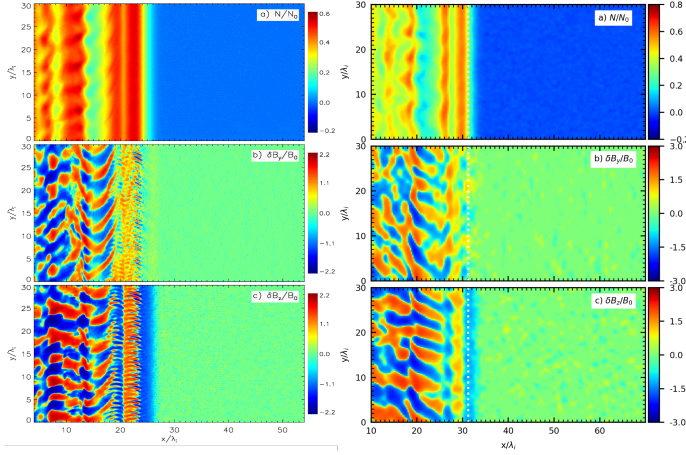


Figure 2: Structure of the shock with $M_s = 3$, $\beta = 5$, and $\theta_{Bn} = 75^\circ$ at time $t\Omega_{ci} = 20$ in the PIC (left) and hybrid (right) simulations. The scaling is logarithmic (see Fig. 1).

in the overshoot in the linear phase. However, strong ion-scale fluctuations, grow in parallel, and their structure in both the PIC and the hybrid simulation is similar, including the development of the waves with $\lambda \sim 5\lambda_i$. In both simulations, ion-scale waves evolve toward multi-scale turbulence, including long-wave shock-front rippling modes (compare Fig. 1a), whose nonlinear wavelengths closely match (not shown). The agreement of our hybrid-kinetic results with the results of the PIC simulations [4–7] proves the validity of the hybrid approach in studying the ion-scale shock physics and the role of ion-scale turbulence in particle acceleration.

Note, that the absence of electron-scale waves in hybrid simulations in the linear stage allows us to observe the early development of fluctuations that later form large-scale shock ripples. Correlations of the magnetic compressive mode structures (B_y) with early density compressions at the shock front, clearly visible in Figures 1a and 2, indicate the importance of the mirror modes in triggering the shock ripples. However, a good match of the linear analysis for AIC waves with nonlinear ripple wavelengths reported in PIC simulations [7, 12] suggests that the effects of the nonlinear evolution of the AIC and mirror modes and nonlinear coupling between these modes are equally important.

3.2 Parameter dependence

Figure 3 compares the structure of shocks with $M_s = 3$ and $\theta_{Bn} = 75^\circ$ in a range of plasma beta: $\beta = 5 - 50$. Figure 4 presents dependence on the shock Mach number, $M_s = 2 - 2.9$, for shocks with $\theta_{Bn} = 75^\circ$ and $\beta = 20$. Figure 5 shows profiles of the ion temperature anisotropy (upper panels, solid lines) and the energy density of magnetic field fluctuations (lower panels) in a range of the shock parameters. In all shocks analyzed here, the reflected ion motion creates ion temperature anisotropies that trigger the growth of ion cyclotron and mirror modes. These waves scatter the ions in pitch angle and reduce their anisotropy, bringing it closer to the upper limit corresponding to marginal stability, given by the condition $T_\perp/T_\parallel - 1 \simeq 1.6/\beta_\parallel^{0.72}$ [13]. These limits are shown with dotted lines in upper panels of Figure 5.

3.2.1 Dependence on plasma β

One can see in Figure 5a, that the temperature anisotropy at the shock front is largely insensitive to the plasma beta. However, higher β values lead to lower marginal stability limits, causing proton

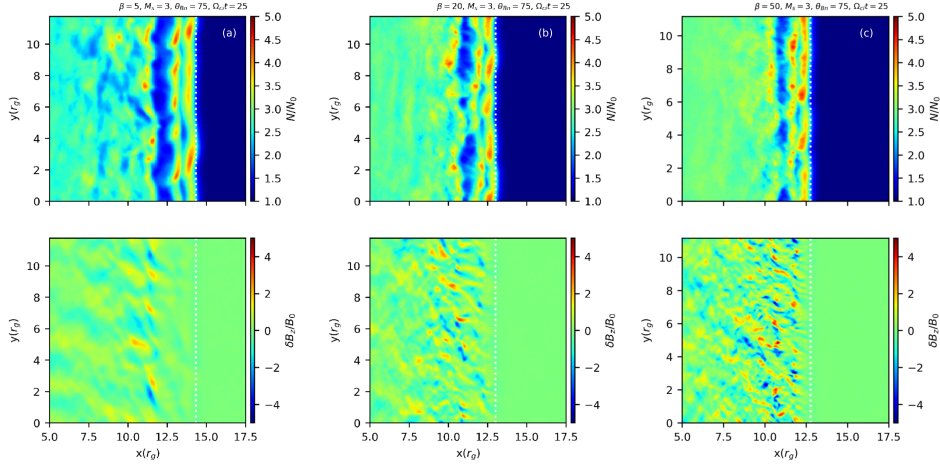


Figure 3: Maps of ion density and B_z magnetic field fluctuations at time $t\Omega_{ci} = 25$ for shocks with $M_s = 3$, $\theta_{Bn} = 75^\circ$, and plasma beta $\beta = 5$ (a), $\beta = 20$ (b), and $\beta = 50$ (c). The scale is linear (compare Fig. 1).

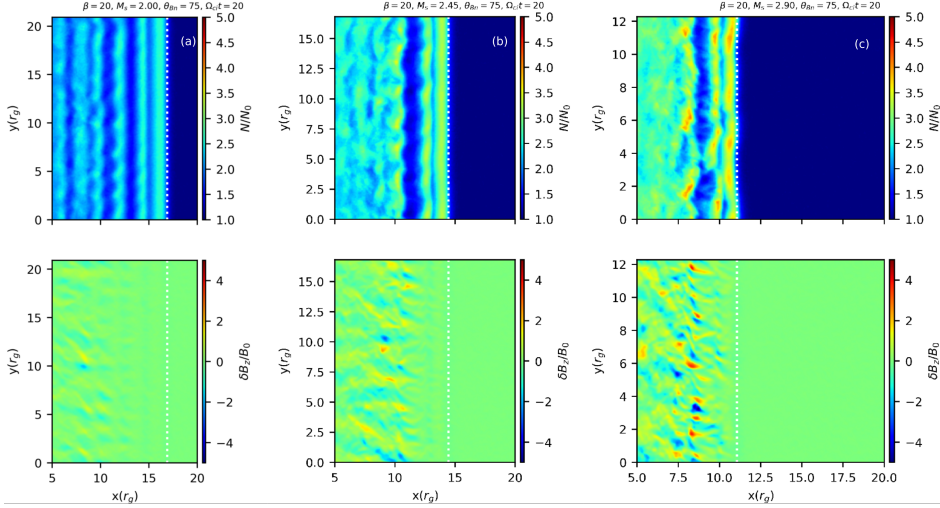


Figure 4: Maps of ion density and B_z magnetic field fluctuations at time $t\Omega_{ci} = 20$ for shocks with $\beta = 20$, $\theta_{Bn} = 75^\circ$, and sonic Mach numbers $M_s = 2$ (a), $M_s = 2.45$ (b), and $M_s = 2.9$ (c).

instabilities to exhibit faster growth rates. In effect, higher- β shocks initially develop stronger turbulence that scatters ions more efficiently, causing the anisotropy to drop faster behind the shock. At high- β shocks the turbulence thus peaks and is confined closer to the shock front (Fig. 3c). Lower- β shocks maintain a finite level of ion isotropy further downstream, where the magnetic energy has also its peak (Figs. 3a-b and 5f). By the simulation time $t\Omega_{ci} = 20$, there is nearly one order of magnitude difference in the total magnetic energy when the plasma beta, varies two orders of magnitude. These observations are consistent with PIC simulation results [14, 15].

3.2.2 Dependence on the sonic Mach Number M_s

The temperature anisotropy at the shock is considerably larger for higher M_s (Fig. 5b), which results in faster growth rates and stronger waves that peak close behind the shock front (Figs. 4c

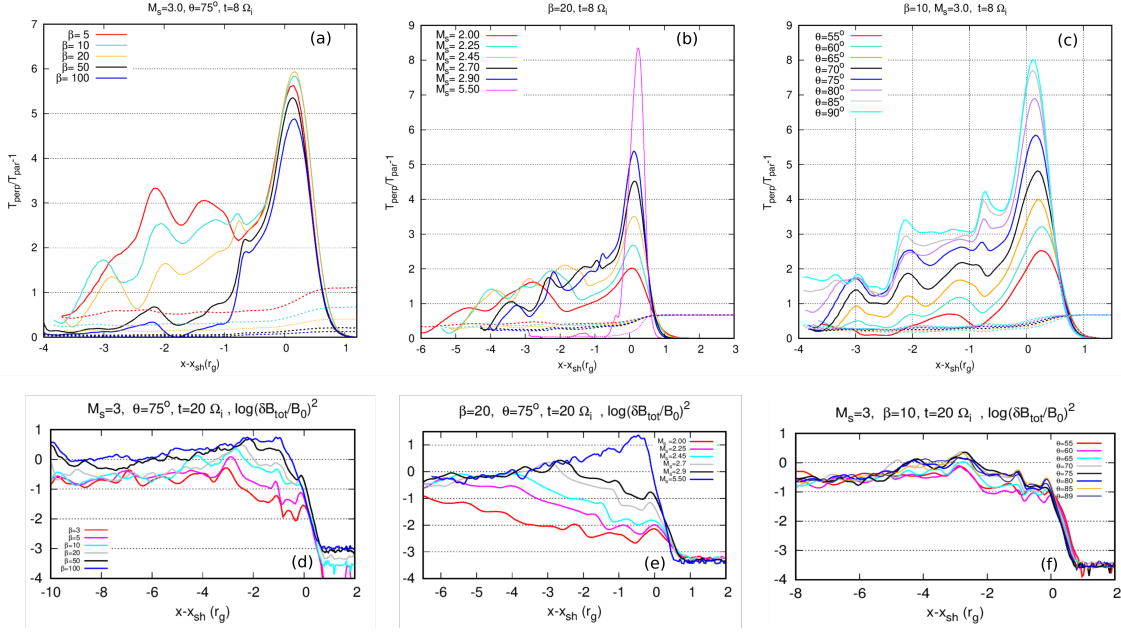


Figure 5: Top row: profiles of the ion temperature anisotropy (solid lines), and the marginal stability condition [13] (dotted lines) at time $t\Omega_{ci} = 8$ and for shocks with different plasma β and $M_s = 3$, $\theta_{Bn} = 75^\circ$ (a), different sonic Mach numbers and $\beta = 20$, $\theta_{Bn} = 75^\circ$ (b), and a range of obliquity angles for $M_s = 3$, $\beta = 10$ (c). Bottom row: the energy density of magnetic field fluctuations for the cases shown in top row, but at $t\Omega_{ci} = 20$.

and 5e). At lower Mach numbers, the waves grow much slower and the turbulence extends further downstream. The amplitude of the magnetic field is two orders of magnitude smaller for the $M_s = 2$ shock, compared to the $M_s \approx 3$ shock. Due to a slow turbulence growth and weak field perturbations, the shock front does not develop ripples [see, e.g., 8, 15].

3.2.3 Dependence on the obliquity angle θ_{Bn}

The temperature anisotropy increases with the obliquity angle, θ_{Bn} , and is a factor of 3.5 smaller at the shock front for $\theta_{Bn} = 55^\circ$, compared to nearly perpendicular shock conditions (Fig. 5c). The energy available for wave generation is thus limited and their growth rates small at low obliquities. The resulting wave amplitudes at low θ_{Bn} angles are smaller compared to higher field inclinations (Fig. 5f). Magnetic fluctuations extend further downstream at low θ_{Bn} , whereas they peak in the second overshoot region for high θ_{Bn} . Inspection of maps (not shown) demonstrates that fluctuations at low- θ_{Bn} shocks evolve towards isotropic turbulence downstream. These shocks develop weaker and longer-wavelength ripples in the shock front density.

4. Summary and outlook

We present preliminary results from our study of the merger shock structures with 2D hybrid kinetic simulations, performed in a wide range of physical parameters, such as the plasma beta, sonic Mach number, and the obliquity angle. Turbulent shock structures in this work match the ion-scale properties described at smaller scales in recent fully kinetic PIC simulations. With our

hybrid approach, we extend these works by investigating large-scale shock systems that allow the development and evolution of broad-band turbulence, up to the largest observed scales of the shock front corrugations. As discussed in Section 1, multi-scale turbulence is critical for efficient electron acceleration through the SSDA process. Our recent PIC simulations demonstrate that the electron-scale structures are less important for electron energization than supra-thermal energies [7]. Thus hybrid kinetic methods are useful for studying the long-time evolution of large-size 2D and 3D systems. Our generalized fluid particle hybrid code is very well suited for this purpose. It also enables the inclusion of additional energetic electron components and the investigation of electron acceleration in turbulent shock structures. Such studies are in progress.

Acknowledgments

The work of S. B. and J. N. has been supported by Narodowe Centrum Nauki through research project no. 2019/33/B/ST9/02569. We gratefully acknowledge Polish high-performance computing infrastructure PLGrid (HPC Centers: ACK Cyfronet AGH) for providing computer facilities and support within computational grant no. PLG/2022/015967. This research was supported by the International Space Science Institute (ISSI) in Bern, through ISSI International Team project #520 (Energy Partition Across Collisionless Shocks).

References

- [1] G. Brunetti and T.W. Jones *Int. J. Mod. Phys. D*, **23** (2014) 1430007.
- [2] D. Krauss-Varban and C.S. Wu *JGR* **94** (1989) 15367.
- [3] S. Matsukiyo, Y. Ohira, R. Yamazaki and T. Umeda *ApJ* **742** (2011) 47.
- [4] X. Guo, L. Sironi and R. Narayan *ApJ* **794** (2014) 153.
- [5] X. Guo, L. Sironi and R. Narayan *ApJ* **797** (2014) 47.
- [6] H. Kang, D. Ryu and J.-H. Ha *ApJ* **876** (2019) 79.
- [7] O. Kobzar, J. Niemiec, T. Amano and et. al. *ApJ* **919** (2021) 97.
- [8] J.-H. Ha, S. Kim, D. Ryu and H. Kang *ApJ* **915** (2021) 18 [2102.03042].
- [9] T. Katou and T. Amano *ApJ* **874** (2019) 119.
- [10] D. Trotta and D. Burgess *MNRAS* **482** (2019) 1154.
- [11] T. Amano *JCP* **366** (2018) 366.
- [12] S. Kim, J.-H. Ha, D. Ryu and H. Kang *ApJ* **913** (2021) 35 [2102.04569].
- [13] S.P. Gary, J. Wang, D. Winske and S.A. Fuselier *JGR* **102** (1997) 27159.
- [14] X. Guo, L. Sironi and R. Narayan *ApJ* **851** (2017) 134.
- [15] X. Guo, L. Sironi and R. Narayan *ApJ* **858** (2018) 95 [1712.03239].